Nanoscale

ROYAL SOCIETY OF CHEMISTRY

PAPER

View Article Online
View Journal | View Issue

Cite this: *Nanoscale*, 2025, **17**, 16239

Effect of kidney disease and vascular calcification on the circulation and distribution of tetracycline-functionalized polymer nanoparticles†

Vanessa Dos Passos Maio, [a,b] Roth-Visal Ung,[b] Karine Greffard,[b] Nicolas Gaudreault, [a,b] Sylvain Picard,[b] Fabrice Mac-Way[b,c] and Nicolas Bertrand *[a,b]

Cardiovascular disease is the leading cause of mortality in patients with chronic kidney disease (CKD), and it is exacerbated by vascular calcification (VC). This pathological deposition of hydroxyapatite in blood vessels leads to arterial and organ dysfunction, yet no effective treatment is currently available. Herein, we developed poly(ethylene glycol)-*b*-poly(lactic acid) (PEG-PLA) nanoparticles functionalized with tetracycline to target VC, given the antibiotic's strong affinity for hydroxyapatite. In rats with CKD, rats with CKD and VC, or healthy animals, we compared the circulation and biodistribution profiles of nanoparticles, as well as the urinary elimination of PEG. Blood and organ analyses revealed similar blood and tissue exposures, with no significant nanoparticle or PEG accumulation in the body. In the same model, we demonstrated that encapsulating vitamin K, a possible inhibitor of VC, alters the pharmacokinetics of the model drug and may enhance its systemic exposure. We employed various methodologies to assess the terminal distribution of nanoparticles in the calcified vascular wall. This work advances our understanding of how kidney disease and vascular calcification can alter the pharmacology of nanoparticles. However, further studies will be necessary to refine tetracycline-based targeting strategies and optimize nanomedicine approaches for VC treatment.

Received 20th March 2025,
Accepted 12th June 2025

DOI: 10.1039/d5nr01158b

rsc.li/nanoscale

1. Introduction

Cardiovascular disease remains the leading cause of mortality in patients with chronic kidney disease (CKD),[1,2] because of comorbidities from traditional cardiovascular risk factors and the contribution of CKD-specific factors, such as vascular calcification.[3,4] Both intimal and medial vascular calcification are prevalent in CKD and are characterized by the pathological deposition of hydroxyapatite ($Ca_{10}(PO_4)_6(OH)_2$) within the vascular lumen, resulting in increased arterial stiffness and organ dysfunction. Indeed, vascular calcification significantly accelerates the progression of coronary artery disease, heart failure, valvular dysfunction, and peripheral vascular disease.[5,6]

Despite the clinical importance of the problem, no drugs are currently approved to treat vascular calcification.[7] Drug repurposing strategies tested in animals and humans include treatments for osteoporosis, notably bisphosphonates[8–10] and denosumab.[11,12] At high concentrations, bisphosphonates inhibit nucleation and growth of hydroxyapatite crystals.[13] However, these drugs generally have poor bioavailability and require dose adjustments in CKD patients. Denosumab, a monoclonal antibody, targets RANKL (receptor activator of nuclear factor-κB ligand), a procalcifying regulator that can be expressed on vascular smooth muscle cells (VSMC).[14,15] Nevertheless, the drug can induce hypocalcemia in CKD patients.[16,17] Importantly, none of these treatments have shown good efficacy in clinical trials, presumably because their high tropism for the skeletal tissue diverts them from their target in the vascular wall.

A strong endogenous inhibitor of calcification in VSMC is the matrix-Gla-protein (MGP).[18] This protein is activated by post-translational γ-carboxylation, a process mediated by Vitamin K.[19,20] Many CKD patients suffer from vitamin K deficiency,[21] and this population has elevated levels of inactive dephosphorylated-uncarboxylated MGP.[22,23] In rat models of CKD, supplementation of vitamin K decreases vascular calcification.[24] However, in CKD patients, the clinical efficacy of vitamin K to decrease vascular calcification remains limited and inconsistent.[25,26] Despite that vitamin K is well tolerated,

[a]*Faculty of Pharmacy, Université Laval, 1050 ave de la Médecine, Quebec City, G1V 0A6, Canada. E-mail: nicolas.bertrand@pha.ulaval.ca; Tel: +1 (418) 525-4444*
[b]*Endocrinology and Nephrology Unit, CHU de Québec-Université Laval Research Center, 2705 Laurier Blvd, Quebec City, G1V 4G2, Canada*
[c]*Département de Médecine, Faculty of Medicine, Université Laval, 1050 ave de la Médecine, Quebec City, G1V 0A6, Canada*

† Electronic supplementary information (ESI) available. See DOI: https://doi.org/10.1039/d5nr01158b

similar to the molecules described above, it does not possess optimal pharmacological properties to reach the vascular wall; vitamin K has low oral bioavailability, and a high volume of distribution, which significantly reduce its concentration in the bloodstream.[27]

Nanomedicines can improve the pharmacological and toxicological profile of drugs by reducing their volume of distribution, prolonging their half-life,[28] and controlling drug release,[29] while minimizing their toxicity and side effects through targeting to specific tissues.[30–33] In this project, we therefore devised ligand-decorated nanomedicines to directly target vascular calcification. As a proof of concept, the intent was to deliver larger amounts of vitamin K to the vascular wall, where it could inhibit calcification. To target nanoparticles, we used tetracycline, a broad-spectrum antibiotic that strongly binds hydroxyapatite, *via* the coordination of oxygen atoms with calcium, hydrogen bonds with phosphate groups, and van der Waals interactions with the inorganic crystal surface.[34] Although tetracycline has no direct effect on calcified tissue, the antibiotic binds bone *in vivo*, as exemplified by its use in bone histomorphometry analyses.[35–37] Tetracycline has been employed as a ligand for bone in various nanomedicines. For example, Wang *et al.* developed two distinct tetracycline-functionalized nanoparticle systems for osteoporosis treatment: poly(lactic-*co*-glycolic acid) (PLGA) nanoparticles[38] and hybrid nanoparticles composed of an amorphous calcium carbonate core coated with phospholipids.[39] In both studies, tetracycline-mediated hydroxyapatite binding was confirmed *in vitro* and *in vivo*. Similar bone-targeting capabilities have been observed with other nanostructures decorated with tetracycline, including PEG (polyethylene glycol)-PLGA[40] and nanoparticles.[41]

In this project, we hypothesized that owing to their ability to remain in the bloodstream for prolonged periods of time,[42] tetracycline-decorated PEG-PLA nanoparticles could distribute to the calcified vascular wall. In the past, nanoparticles decorated with peptides[43,44] and antibodies[45–47] showed their ability to bind targets within the vasculature. Small molecular weight ligands do not usually compromise the circulation times of nanoparticles, contrary to some peptides or proteins, and are easier to manufacture.[48] We therefore explored the biological fate of long-circulating tetracycline-targeted polymer nanoparticles, in models of CKD with vascular calcification.

For this purpose, we employed the rat 5/6 nephrectomy model, in conjunction with a calcifying diet.[36] Our objective was to evaluate the biodistribution and pharmacokinetics of tetracycline-functionalized nanoparticles and vitamin K, under conditions of impaired renal function and vascular calcification.

2. Materials and methods

DL-Lactide (Acros Organics, Morris Plains, USA) was crystallized twice from ethyl acetate and dried under reduced pressure. *tert*-Butyloxycarbonyl amine polyethylene glycol hydroxyl (7500 g mol^{-1}; *t*-boc-PEG$_{7.5k}$) was obtained from Jenkem Technology (Beijing, China). Poly(lactic-*co*-glycolic acid) 95 000 g mol^{-1} (PLGA$_{95k}$) was from Corbion Purac (Gorinchem, The Netherlands). Acid acetic, benzoic acid, *N*,*N*-diisopropylethylamine (DIPEA), succinic anhydride, tetracycline hydrochloride, triazabicyclodecene (TBD) and zinc acetate dihydrate were procured from Sigma-Aldrich (St Louis, USA). *N*,N′-Dicyclohexylcarbodiimide (DCC), 4-dimehylaminopyridine (DMAP) and hydroxyapatite were from Acros Organics (Morris Plains, USA). Vitamin K1 (phytonadione) and trifluoroacetic acid were purchased from Alfa Aesar (Tewksbury, USA). Solvable™ aqueous based solubilizer and Hionic-Fluor™ liquid scintillation cocktail were procured from PerkinElmer (Waltham, USA). CytoScint™ liquid scintillation cocktail was obtained from MP Biomedicals (Irvine, USA). Isotonic phosphate buffered saline pH 7.4 solution (PBS) was prepared from Bio Basic PBS 10× (Markham, Canada). Acetonitrile, dichloromethane, diethyl ether, dimethyl sulfoxide (DMSO), ethanol, ethyl acetate, methanol, 30% (w/w) hydrogen peroxide, tetrahydrofuran (THF), and all other materials were purchased from Fisher Scientific (Fair Lawn, USA) unless specified otherwise.

2.1 Tetracycline-PEG-PLA (Tet$_1$-PEG-PLA) polymer synthesis

Polyethylene glycol-*block*-polylactic acid (PLA-PEG) was synthesized by ring-opening polymerization of D,L-lactide at room temperature using *t*-Boc-PEG-OH as an initiator, and TBD as a catalyst.[49] Briefly, *t*-Boc-amine-PEG$_{7.5k}$-OH (0.06 mmol, 1 eq.; 0.46 g) and lactide (10.9 mmol, 182 eq.; 1.54 g), previously dried under vacuum overnight, were dissolved under an inert atmosphere in 5.5 mL of anhydrous dichloromethane. The catalyst, TBD (1.1 mmol, 18 eq.; 0.15 g) was dissolved in 1 mL of dichloromethane and added to the reaction. The mixture was polymerized at room temperature for 30 minutes and quenched by adding benzoic acid (5.5 mmol, 92 eq.; 0.65 g). The terminal amine was deprotected by removal of the protecting group in 5.5 mL anhydrous dichloromethane containing 5 mL of trifluoroacetic acid, at 0 °C for 1 hour. The solution was concentrated and precipitated in cold diethyl ether. The product was dried overnight under vacuum. Next, the addition of a carboxyl group was made at 35 °C. The precipitate was dissolved in 3 mL of dichloromethane and excesses of succinic anhydride (10 eq.; 0.36 g), also dissolved in 3 mL of dichloromethane, and DIPEA (2 eq.; 200 μL) were added. After 3 h, the solution was concentrated and precipitated in cold diethyl ether. The product was dried overnight under vacuum. Tetracycline was added to PEG-PLA copolymer by esterification reaction between the carboxyl group of PEG and one hydroxyl group of tetracycline in the presence of DCC and DMAP (molar ratio, PEG-PLA/DCC/DMAP = 1 : 47 : 29). Briefly, PEG-PLA copolymer (0.7 g) and DCC (0.40 g) were dissolved in 5 mL of anhydrous dichloromethane. The solution was stirred at room temperature for 20 minutes to activate the carboxylic acid of PEG-PLA conjugates. DMAP (0.15 g) were dissolved in 1 mL of anhydrous dichloromethane and then added to the reaction mixture. Right after, tetracycline hydrochloride (0.20 g) (molar ratio, Tet/PEG-PLA = 1 : 5), dissolved in DMSO was added, the reaction continued for another 16 h. DCU crystals were

removed by filtration. The solvent was removed by rotary evaporation, and the polymer was precipitated thrice in cold methanol and dried over vacuum. The product of each step of the synthesis was analyzed by ^{1}H-NMR spectroscopy and by gel permeation chromatography (GPC), as reported in the ESI.†

2.2 Preparation of nanoparticles

Targeted tetracycline nanoparticles (Tet-NP) and non-targeted nanoparticles (NP) were prepared by nanoprecipitation from acetonitrile solutions.[50] Briefly, tetracycline-PEG-PLA or PEG-PLA polymer solution was mixed with a PLGA solution as per the ratio described in ESI Table 2,† to obtain a total volume of 1 mL, and then added dropwise to 9 mL of water under stirring (1600 rpm; 2 min). The polymer mixture was modified to obtain particles with different quantities of the tetracycline ligand (10 to 80 wt% of Tet_1-PEG-PLA). To enable tracking of nanoparticles *in vitro* and *in vivo*, a [^{14}C]-$PLGA_{20k}$ copolymer (Moravek Biochemicals, Brea, USA) or a fluorescent [Cy5.5]-PLA_{20k} or [Cy5]-PLA_{20k} polymer (synthesized as described in ESI†) were integrated into the polymer mixtures. For the preparation of vitamin K-loaded nanoparticles (Tet-NPK or NPK), 70 μL of a 15 mg mL^{-1} ethanolic solution of this vitamin was evaporated under nitrogen (35 °C), in a glass vial protected from light. After, the polymer precursor solutions were mixed into this vial, and the nanoparticles were obtained by nanoprecipitation, as above. To remove unencapsulated vitamin K, the nanoparticle suspension was purified by solid phase extraction (SPE) on a Strata®-X 33 μm polymeric reversed phase 200 mg per 6 mL column (Phenomenex, Torrance, USA). Briefly, the sorbent was initially conditioned with 4 mL of methanol, followed by 4 mL of water. The nanoparticle suspension (10 mL) was then introduced into the cartridge, and elution was performed using a syringe. Subsequently, all nanoparticle formulations were washed five times with water using an Amicon® ultrafiltration device (molecular weight cut-off: 100 000) from Millipore (Carrigtwohill, Ireland). Each wash was standardized to achieve a ten-fold dilution, ensuring a very low organic solvent content in the final formulation.[51]

2.3 Characterization of nanoparticles

The nanoparticle size (*Z*-average) and size distribution (polydispersity index – PDI) were measured before and after purification by dynamic light scattering (DLS), at 22 °C with a 173 backscatter angle, using a Malvern Zetasizer Nano S (Malvern Instruments, Westborough, MA). Nanoparticle concentration was determined by gravimetry. Vitamin K loading was measured by high performance liquid chromatography (HPLC) with a diode-array detector (DAD), as described in the ESI.† A table presenting the composition and characteristics of each nanoparticle used is provided in the ESI section.†

2.4 Targeted tetracycline nanoparticles binding on hydroxyapatite *in vitro* and *ex vivo*

Nanoparticles were prepared with [^{14}C]-PLGA and with different quantities of Tet_1-PEG-PLA polymer (10–80 wt%) as describe above. A fixed amount of radiolabeled nanoparticles was incubated with increasing amounts of hydroxyapatite in PBS, at 37 °C with constant agitation for 1 h. After low-speed centrifugation (2 min; 120 g), the radioactivity content in 100 μL of supernatant was measured on a scintillation counter (300 SL TDCR LSC, Hidex, Finland) using 8 mL of CytoScint™ scintillation fluid. The percentage of nanoparticles bound was determined by the difference between the total amount of radioactivity added into the tube and the radioactivity content of the supernatant after the incubation, multiplied by 100. To verify the stability of the tetracycline ligand, radiolabeled nanoparticles with 80 wt% of Tet_1-PEG-PLA polymer were prepared. These nanoparticles were stored in water at 4 °C and the same incubation test was repeated after 1 and 3 weeks of storage. The nanoparticles' size (*Z*-average) and the polydispersity index (PDI) were also measured at time zero, and after three weeks, as described in 2.3. Targeted and non-targeted nanoparticles labeled with PLA-Cy5.5 were incubated with calcified rat abdominal aorta sections (110–130 mg) for 1 hour in PBS, with shaking, at 37 °C. After incubation, the supernatant was removed following centrifugation (2 minutes at 120 g), and the aortas were washed three times with PBS. Next, aorta images were captured using an IVIS Lumina II optical system with an excitation wavelength of 640 nm and an emission filter for Cy5.5.

2.5 The rat model of chronic kidney disease with vascular calcification (CKD + VC)

All animal studies were conducted following the guidelines of the Canadian Council of Protection of Animals, and were approved by the Animal Care Committee of the University Laval. Seven-week-old male Wistar rats weighing 200–225 g (Charles River, Saint-Constant, Canada) were allowed free access to food and water in temperature and humidity controlled conditions, with a 12 h dark/light cycle. Chronic kidney disease (CKD) was induced by subtotal renal mass reduction (5/6 nephrectomy) that consisted of the resection of the upper and lower poles of the left kidney, followed, 1 week later, by right nephrectomy.[36] To induce VC, animals were given a calcifying diet with high calcium (1.2%) and phosphate (1.2%) (Envigo, Indianapolis, USA), combined with subcutaneous injections (0.5 μg kg^{-1}; 3 times per week) of calcitriol (1α,25-dihydroxyvitamin D3; Sigma-Aldrich, St Louis, USA). This calcifying diet was initiated two weeks after the right nephrectomy. The health status of CKD + VC rats was monitored daily by veterinary technicians (general appearance, mobility, and grooming habits). Animals were considered to have developed vascular calcifications when their general condition deteriorated and when they lost weight for two consecutive weeks. After the sacrifice, to characterize the CKD induction, serum calcium, phosphorus, and creatinine, were determined by an autoanalyzer system (Ilab 1800, Lexington, MA, USA). Post-mortem von Kossa staining was used to quantify vascular calcification. Briefly, a thoracic aorta segment was fixed for 24 h, dehydrated, and embedded in paraffin as previously described. Sections with thicknesses of 5 μm were deparaffinized and

rehydrated before staining with 5% silver nitrate and light exposure, followed by 5% sodium thiosulphate addition and counterstained with nuclear fast red solution. Quantification was performed on the whole thoracic segment at a magnification of 20× using the ImagePro-Plus analysis software (Media Cybernetics, Silver Spring, MD, USA).

2.6 PEG excretion and biodistribution study

An *in vivo* study was carried out to verify whether reduced renal function, in the CKD + CV rat model, could have an impact on the excretion of this polymer. Three groups of animals were studied: (1) CKD rats + calcifying diet + calcitriol (CKD + VC), (2) CKD rats + normal diet (KD) and (3) healthy rats + normal diet (Healthy). Five to six animals were included in each group. Fifteen weeks after the right nephrectomy, each rat received 135 μg of [^{14}C]-labeled PEG_{10k} (synthesized as described in ESI†) in a DPBS solution (Wisent Bioproducts, Canada) and was placed in individual metabolic cages. Urine samples were collected after 4, 8, 18, and 24 h. After the last sampling point, the animals were sacrificed, and the organs were collected. All samples were assessed by scintillation counting, using Hionic Fluor® as a scintillation cocktail. Urine samples were analyzed directly, while organs were digested for at least 48 h, at 60 °C, in Solvable® and bleached with 30% hydrogen peroxide, prior to analysis.

2.7 Pharmacokinetics studies of targeted tetracycline nanoparticles

In the pharmacokinetics studies, all formulations were injected *via* the subclavian vein under isoflurane anesthesia (2.5%). Approximately 200 μL blood samples were collected in EDTA coated capillary tubes by the lateral saphenous vein, at fixed intervals. The last blood sample was collected under anesthesia by heart puncture. The animals were then sacrificed, organs were flushed with PBS and collected for analysis.

To study the pharmacokinetic profile of blank targeted tetracycline nanoparticles (Tet-NP) in rats with different health status, three groups of animals were studied: (1) CKD rats + calcifying diet + calcitriol (CKD + VC), (2) CKD rats + normal chow (CKD) and (3) healthy rats + normal chow (Healthy). Fifteen weeks after the 5/6 nephrectomy, each rat received 4 mg of [^{14}C]-labeled Tet-NP, containing 50% of Tet1-PEG-PLA polymer (complete composition shown in ESI Table 5†). Blood samples were collected after 15, 30 min, 1, 2, 4, 6, and 12 h post-dosing. Five to six animals were included in each group. Blood and organ samples were digested for at least 48 h, at 60 °C, in Solvable®, bleached with 30% hydrogen peroxide, and assessed by scintillation counting, using Hionic Fluor® as a scintillation cocktail.

For the pharmacokinetic profile of vitamin K-charged tetracycline nanoparticles (Tet-NPK containing 80% of Tet_1-PEG-PLA polymer), the CKD + VC was induced in a group of rats as described above. When animals experienced decreases in body weight for two consecutive weeks it was deemed that they had developed VC, and they were randomised to three groups, according to their weight. Five to twelve rats were included in each group. The first group received the equivalent of 1 mg of vitamin K encapsulated in targeted nanoparticles (Tet-NPK, approximately 10–12 mg of nanoparticles, n = 12), the second received the same dose of this vitamin encapsulated in non-targeted nanoparticles (NPK, approximately 10–12 mg of nanoparticles, n = 11), and the third also received 1 mg of vitamin K from a commercial formulation (10 mg mL^{-1} Phytonadione Injectable Emulsion USP; Sandoz, Boucherville, Canada) (Free K, n = 5). The nanoparticles were labeled with fluorescent Cy5.5-PLA (nanoparticles composition details are shown in ESI Table 5†). Blood samples were collected after 15, 30 min, 1.5, 3, 6, 12, 24 and 48 h post-dosing. Plasma was separated by centrifugation (3000*g* for 15 min) at 4 °C, then stored protected from light at −80 °C. Right after the sacrifice, the organs were imaged by IVIS and stored at −80 °C. The vitamin K content in plasma was assayed by HPLC after protein precipitation. Briefly, 25 μL of plasma was supplemented with 45 μL of acetonitrile. The tube was vortexed for 10 seconds. Next, 45 μL of ethanol was added, and the tube was vortexed for 10 seconds again. The sample was sonicated for 30 min and centrifuged for 30 min (3000*g*; 22 °C). An aliquot of the supernatant was then analyzed by HPLC using the method with zinc reduction and fluorescence detection, described in the ESI.†

2.8 Calculation of pharmacokinetics parameters

For the study with blank targeted tetracycline nanoparticles, the PK parameters were calculated using nanoparticles concentration, expressed in percentage of injected dose per gram of blood (%ID g^{-1}) *versus* time profiles, and for the study with Tet-NPK, they were calculated using vitamin K plasma concentration in g mL^{-1} *versus* time profiles. PK data were treated by non-compartmental analysis. Maximal concentration (C_{max}) corresponds to the maximum concentration measured. The apparent first-order terminal elimination rate (K_e) was estimated with a linear least-squares regression on the semi-log plot of the concentration *versus* time curve using the last 3 points of the curve. The areas under the concentration *versus* time curve (AUC_{0-t}) were calculated by the trapezoidal method. Areas under the plasma concentration *versus* time curve from time zero to infinity ($AUC_{0-\infty}$) were calculated by adding AUC_{0-t} to the ratio of the last measurable concentration to K_e. Extrapolated volume of distribution (V_d) was determined by dividing the injected dose by time zero concentration (C_0). Terminal elimination half-life ($t_{1/2}$) was assessed as $\ln(2)/K_e$. Total clearance (CL) was quantified as the injected dose divided by $AUC_{0-\infty}$.

2.9 Statistical analysis

Values are presented as the mean ± standard deviation (SD). Statistics were computed with GraphPad Prism 7. Comparison of the experimental data was carried out by one-way analysis of variance (ANOVA), using Tukey as a *post-hoc* test to determine the significance of all paired combinations. A value of $p < 0.05$ was considered significant.

3. Results

3.1 Tetracycline-PEG-PLA polymer and nanoparticles

A PEG-PLA diblock copolymer was synthesized by D,L-lactide ring-opening polymerization using *t*-Boc-PEG-OH as the initiator, and TBD as the catalyst.[49] Fig. 1A illustrates the four-step synthesis process. After PEG-PLA polymerization, the *t*-Boc protecting group was removed *via* TFA hydrolysis.[52,53] The resulting terminal primary amine was reacted with succinic anhydride to yield a carboxylic acid-terminated PEG block. A tetracycline molecule was conjugated to the PEG chain *via* an ester bond in the final step. ^{1}H-NMR spectra and GPC ana-

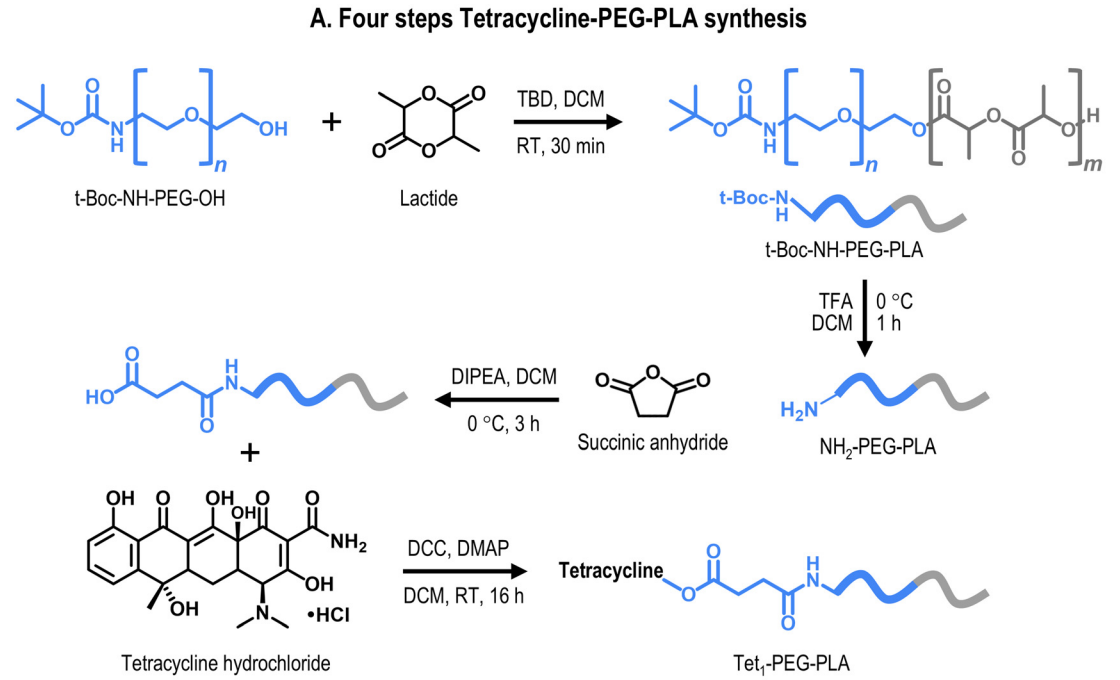

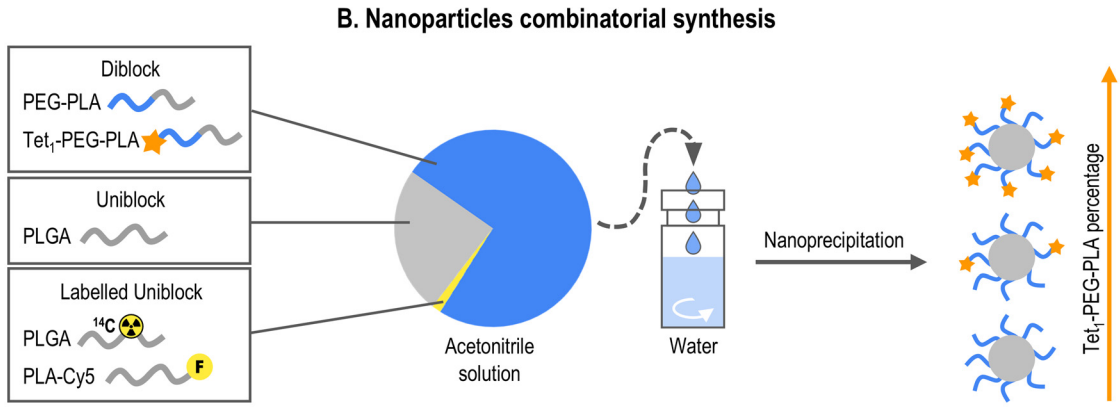

C. Nanoparticles size characterization

Tet_1-PEG-PLA (wt%)	PEG-PLA (wt%)	PLGA (wt%)	Size (nm)	PDI
80%	0%	20%	114 ± 3.4	0.105 ± 0.011
75%	5%	20%	101 ± 1.5	0.094 ± 0.013
50%	30%	20%	95 ± 1.8	0.095 ± 0.018
20%	60%	20%	98 ± 0.5	0.105 ± 0.011
10%	70%	20%	95 ± 1.2	0.081 ± 0.013
0%	80%	20%	86 ± 0.3	0.089 ± 0.017

Mean ± SD

Fig. 1 Targeted (with tetracycline) and non-targeted PEG-PLA nanoparticles were prepared and characterized. (A) Synthesis route of Tet_1-PEG-PLA. (B) Combinatorial synthesis of nanoparticles by nanoprecipitation using different percentages of Tet_1-PEG-PLA. (C) Nanoparticles' size (*Z*-average) and polydispersity index (PDI) measured by dynamic light scattering (DLS).

lysis results for each product at every synthesis step are provided in the ESI section.†

Nanoparticles were prepared by nanoprecipitation.[42] In this method, polymers are dissolved in acetonitrile, a solvent miscible with water, and are added dropwise to water. The solvent diffuses out, while the polymers collapse, forming nanoparticles that can encapsulate drugs.[50] To prepare targeted tetracycline nanoparticles, the Tet_1-PEG-PLA diblock copolymer was mixed with PLGA in varying proportions (10 to 80 wt% of Tet_1-PEG-PLA). Control, non-targeted nanoparticles were also prepared, using an equivalent PEG-PLA diblock polymer without tetracycline. Depending on the test performed, amounts of either ^{14}C-PLGA or PLA conjugated to a fluorochrome (Cy5 or Cy5.5) were added to the polymer mixture, prior to nanoprecipitation to enable nanoparticle tracking (Fig. 1B). A table detailing the composition and characteristics of each nanoparticle used is available in the ESI section.†

The resulting non-targeted nanoparticle suspensions exhibit a translucent whitish appearance, whereas the targeted tetracycline nanoparticles are translucent with a yellowish-brown tint due to the presence of tetracycline. The combinatorial synthesis approach—where nanoparticles are prepared by systematically varying a single parameter[42,54] – allowed to prepare nanoparticles with increasing quantities of Tet_1-PEG-PLA polymer. Both non-targeted and targeted tetracycline nanoparticles displayed an average diameter (*Z*-average) of approximately 100 nm and showed a low polydispersity index (PDI) (Fig. 1C).

3.2 Targeted tetracycline nanoparticles bind hydroxyapatite

We used ligand-dependent precipitation[52] to evaluate how targeted tetracycline nanoparticles could bind to inorganic hydroxyapatite ($Ca_{10}(PO_4)_6(OH)_2$). Here, radioactive targeted and non-targeted nanoparticles were incubated for 1 h in PBS, with increasing amounts of hydroxyapatite microparticles (with a diameter of 5–50 μm). Upon centrifugation of the hydroxyapatite, only unbound nanoparticles remained in the supernatant. Fig. 2 shows that, as the content of Tet_1-PEG-PLA polymer in the nanoparticle increases, nanoparticles bind progressively more to the inorganic crystals. For example, nanoparticles containing 80 wt% of Tet_1-PEG-PLA polymer bound to hydroxyapatite approximately 3-fold more than nanoparticles prepared with 20 wt% of the targeted polymer (83.9% *vs*. 28.1%, $p < 0.05$) (Fig. 2A). As the quantity of hydroxyapatite increases from 1.6 to 6.4 mg, the residual quantities of nanoparticles remaining in the supernatant decrease for all tetracycline-containing nanoparticles. The interactions between nanoparticles and hydroxyapatite can be observed by IVIS imaging when targeted and non-targeted fluorescent nanoparticles were incubated with hydroxyapatite (Fig. 2A). Here, tetracycline-functionalized nanoparticles are collected on the hydroxyapatite pellet, while their non-targeted counterparts remain in suspension.

Next, we tested whether targeted tetracycline nanoparticles remained stable during storage (three weeks in water, at 4 °C). This is helpful to understand if nanoparticles can be stored before being used. During that period, dynamic light scattering (DLS) measurements did not show significant variations in size and size distribution (Fig. 2B). This agrees with previous results obtained by our group,[55] demonstrating that the colloidal stability of PEG-PLA nanoparticles is minimally affected by storage in water at 4 °C. Here, given the presence of the targeting ligand, it was also important to establish that storage did not result in the hydrolysis of the tetracycline moiety. Hence, Fig. 2B shows that storage does not appear to affect interactions between targeted tetracycline nanoparticles and hydroxyapatite over time. In all conditions tested, fresh and aged nanoparticles maintained the same ability to bind hydroxyapatite (Fig. 2B).

To test the ability of the nanoparticles to bind to hydroxyapatite crystals from biological origin, fluorescent nanoparticles (labeled with PLA-Cy5.5) were incubated with sections of calcified rat aorta. Images taken by IVIS showed noticeable fluorescence, even after three PBS washes, indicating that the nanoparticles can interact with the crystals in aortic tissue. Fig. 2C shows representative images of *ex vivo* interactions, at two nanoparticle concentrations (20 and 80 μg mL^{-1}), showing an approximately 3-fold increase in tissue fluorescence for the targeted formulation compared to its non-targeted counterpart.

We also established that surface functionalization with tetracycline did not alter internalization by normal and calcified human aortic smooth muscle cells (HASMC). This was assessed by flow cytometry, as described in the ESI,† using fluorescent nanoparticles. For targeted and non-targeted nanoparticles, the proportion of Cy5-positive cells increased in a dose-dependent manner. The half maximal concentration (EC_{50}) calculated for targeted and non-targeted nanoparticles was similar, ranging between 1.0–1.4 μg mL^{-1}, for normal and calcified HASMC (Fig. 2D). This is important because it shows that the differences in the physicochemical properties of the nanoparticles do not significantly affect interactions with living cells.

3.3 Induction of chronic kidney disease and vascular calcifications in rats

One common preclinical model of chronic kidney disease (CKD) involves surgically removing five-sixths of the kidneys (*i.e.*, 5/6 nephrectomy). In this procedure, two-thirds of one kidney are surgically removed, followed, one week later, by the removal of the second kidney.[36,56–58] This CKD model has more than 40% decrease in creatinine clearance (*i.e.*, reduced renal function),[57,59] and increased urine production due to dysfunctional water reabsorption.[59] In the model, vascular calcification can be induced by feeding animals with a calcifying diet supplemented by subcutaneous calcitriol injections. Vascular calcification occurs due to biochemical alterations such as hyperphosphatemia and hypercalcemia in a uremic environment.[36,57] Beyond vascular calcification, animals also suffer from bone turnover and microarchitecture anomalies typical of CKD-mineral and bone disorders.[36,60]

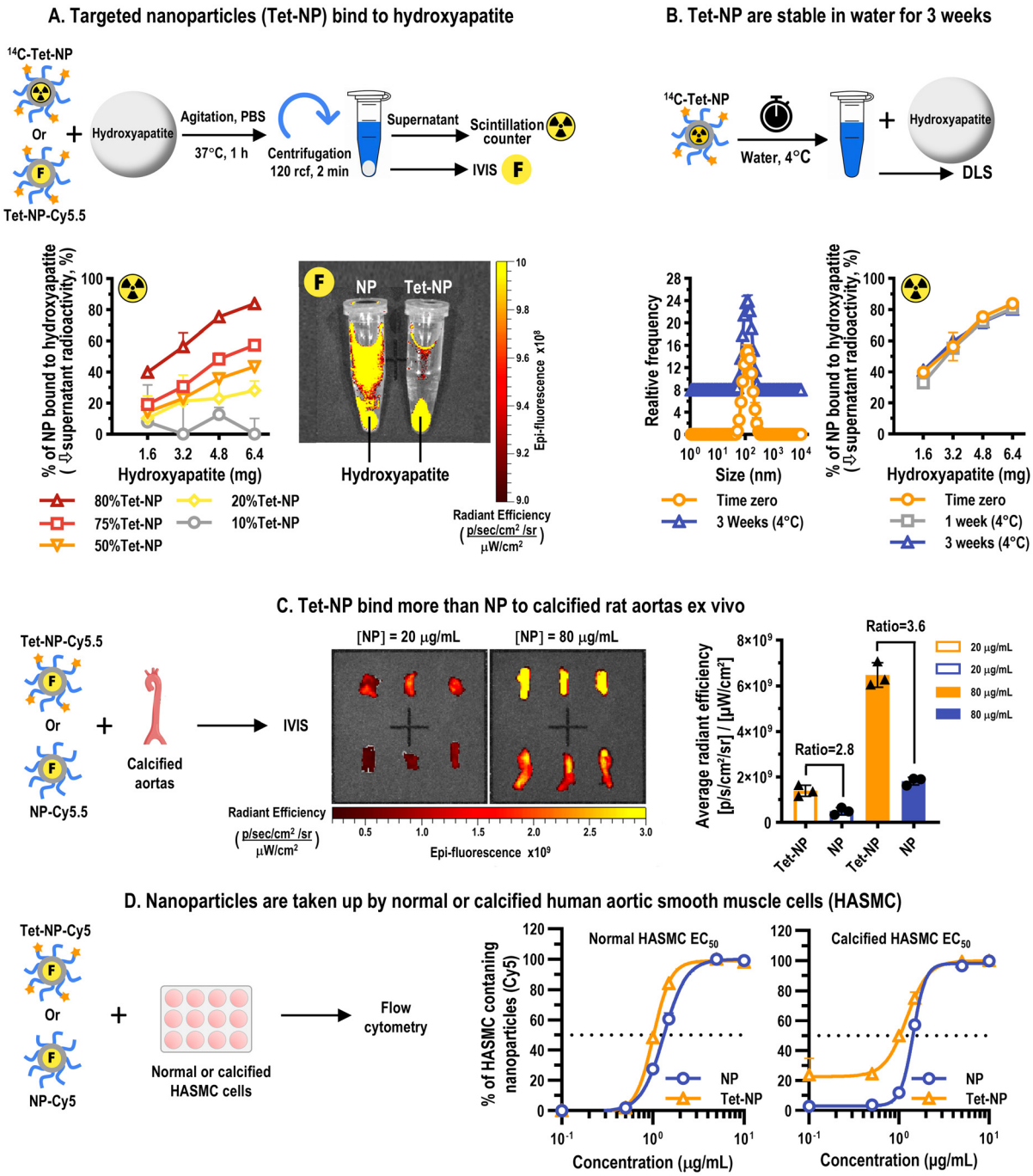

Fig. 2 The presence of tetracycline increases the binding between nanoparticles and hydroxyapatite. A. Tet-NP with different quantities of the Tet_1-PEG-PLA polymer (10–80 wt%) were tested. (B) Tet-NP with 80 wt% of Tet_1-PEG-PLA exhibited a similar binding profile to hydroxyapatite and maintained a similar size after 3 weeks of storage in water at 4 °C. (C) IVIS images show that Tet-NP biding more than non-targeted nanoparticles (NP) to hydroxyapatite microcrystals. (D) The half-maximal concentration (EC_{50}) calculated for Tet-NP and NP was similar in both normal and calcified cells. Values represent mean ± SD (n = 3).

The overall health status of the animals was monitored daily. The progression of vascular calcification was evaluated on a 7-days basis, by weighing animals. Fig. 3A demonstrates that healthy animals (control) exhibit normal growth; throughout the 16 weeks of weight monitoring, they reached an average body weight of 526 ± 46 g. As expected, in the first weeks of the protocol, the two groups that underwent 5/6 nephrectomy (CKD and CKD + VC) showed less weight gain than the control group. After this convalescence phase, their growth returned to normal, reaching an average weight of 494 ± 43 g and 468 ± 38 g at the end of the study, for the CKD and CKD + VC groups respectively. By the 15th week of monitoring

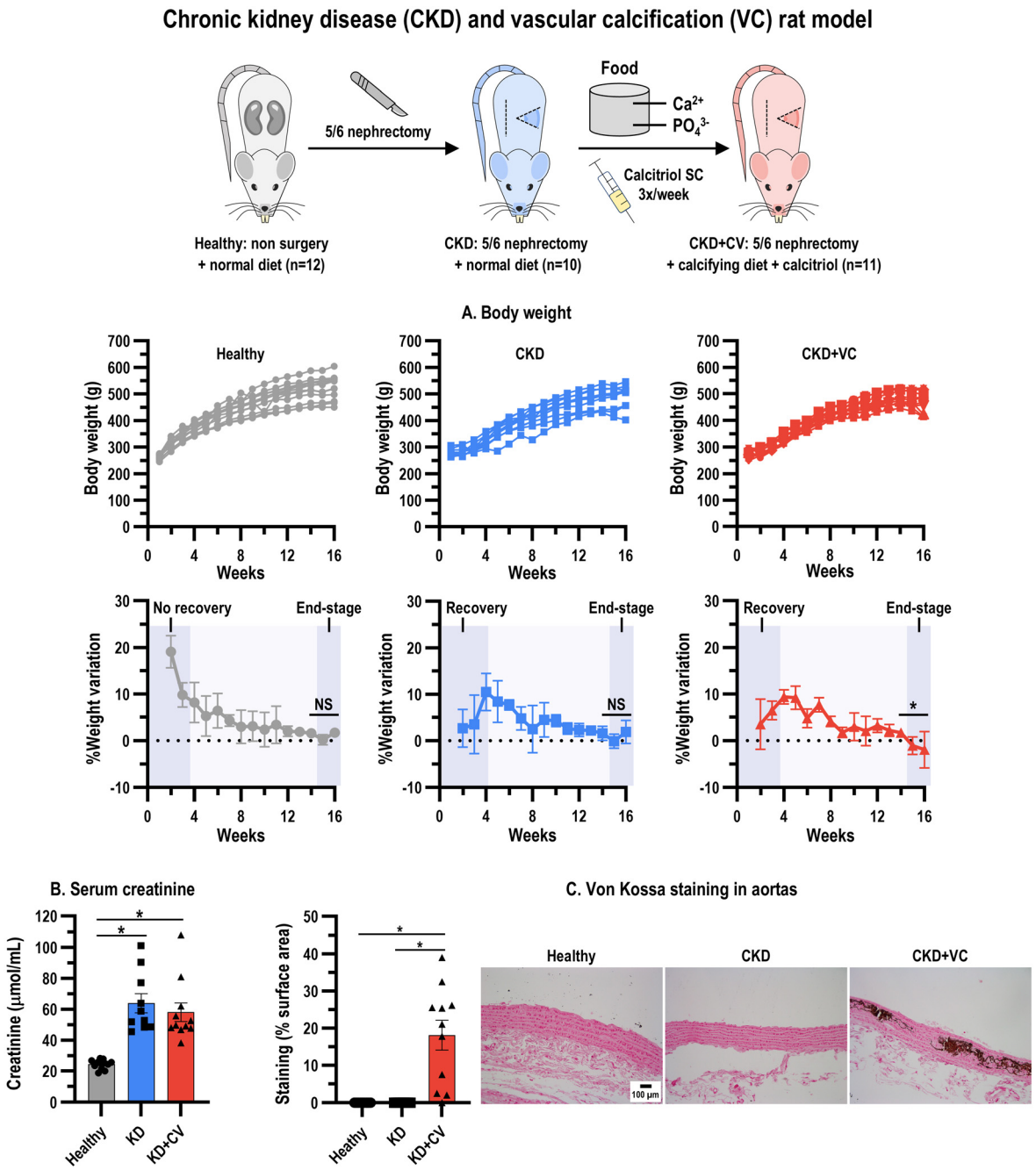

Fig. 3 Rats subjected to 5/6 nephrectomy and given a calcifying diet supplemented with subcutaneous (SC) calcitriol injections developed medial vascular calcification (VC). (A) A significant difference in weight loss was observed for the CKD + VC group. (B) CKD and CKD + VC groups showed increased creatinine values 14 weeks after the 5/6 nephrectomy. (C) Only the CKD + VC group showed calcifications in the aorta. Values represent mean ± SD for *n* animals. NS: no significant difference ($p > 0.05$ as determined by ANOVA with Tukey's *post-hoc* test).

(end-stage period), animals on a calcifying diet developed vascular calcification and began to lose weight. The weight loss in the last two weeks for the CKD + VC group was significant, reaching 3% of their last measure, compared to a weight gain of 2% in the CKD and the healthy group. This deterioration of the health status indicated that vascular calcification had progressed significantly and indicated the right time to start experiments with nanoparticles.

Postmortem biochemistry analysis showed that nephrectomised animals had a significant increase in serum creatinine values compared with the control group (Fig. 3B). Kidney function was comparable between CKD groups receiving a normal and calcifying diet, and was 2.5-fold higher than those in the control group. Likewise, von Kossa staining was carried out to detect calcifications present in the thoracic aorta. We observed that only the

CKD + VC group developed extensive calcification of the vascular tissue (Fig. 3C).

Of the 24 rats included in the initial 5/6-nephrectomy groups, two died during the week following the second surgery, and a third rat, from the CKD + VC group, died in the fifteenth week. After 16 weeks of monitoring, each group was subdivided to conduct two studies: (1) excretion and biodistribution of PEG, and (2) pharmacokinetics and biodistribution of targeted nanoparticles.

3.4 Impact of chronic kidney disease on the excretion of PEG and the pharmacokinetics of nanoparticles

Renal excretion is the main route of elimination for PEG, a synthetic polymer that is not biodegradable.[61] In animals with normal kidney function, Yamaoka *et al.* (1994), established that linear PEG chains with a molecular weight below 20 000 g mol^{-1} were freely filtered by the renal glomerulus.[62] Here, we were interested in determining whether a decrease in kidney function affects the elimination of the polymer. Using the animal models described above (healthy, CKD, and CKD + VC rats), we investigated the urinary excretion of a 10 000 g mol^{-1} [^{14}C]-PEG molecule.[63] We intravenously injected 135 μg of [^{14}C]-PEG to animals housed in metabolic cages (0.5 μCi per animal) and collected urine over a period of 24 h.

The total 24 h urine volume collected was similar between groups, although greater variability was observed in the nephrectomized animals (Fig. 4). Healthy rats excreted approximately 11 ± 2 mL, while 35 ± 23 mL and 26 ± 14 mL were collected from the CKD and CKD + VC animals, respectively. The kinetics at which radioactive PEG was excreted in the urine was also comparable between groups, with *ca.* 50% of the injected dose recovered within the first 4 h. Over 24 h, the fraction of the PEG injected dose recovered in the urine was greater than 80% for all animals, without significant differences observed between the groups (Fig. 4). After euthanasia, the biodistribution of [^{14}C]-PEG was evaluated and less than 6% of the injected dose was found in the principal organs 24 h after injection (Fig. 4). The principal organs where radioactivity was recovered were the liver and the kidneys (*i.e.*, the residual kidney tissue in nephrectomised animals). These results indicate that limited accumulation of PEG occurs in rats, even with a drastic reduction in renal function. Likewise, the presence of vascular calcification does not appear to affect PEG excretion.

Next, we investigated whether the animals' health status and the reduction in renal function affected the circulation of targeted tetracycline nanoparticles in the bloodstream. To do so, pharmacokinetic and biodistribution profiles were determined. Specifically, a single dose of targeted tetracycline nanoparticles (4 mg per rat), containing 50 wt% Tet_1-PEG-PLA polymer and radiolabeled with [^{14}C]-PLGA, were injected into three groups of rats: (1) control group, with healthy animals; (2) animals with chronic kidney disease (CKD) and, (3) animals with chronic kidney disease and vascular calcification (CKD + VC).

Fig. 5 shows the profiles of mean blood concentration *vs.* time, for the three groups of animals. This data shows very similar circulation profiles without any significant differences in pharmacokinetic parameters, including maximum concentration (C_{max}), the time at which maximum concentration is observed (t_{max}), the area under the blood concentration *vs.* time curve ($AUC_{0-24\ h}$), the half-life ($t_{1/2}$), the volume of distribution (V_d), and the clearance (CL). The lack of differences was anticipated as the diameter of these nanoparticles was significantly higher than the hydrodynamic cut-off of glomerular filtration (*i.e.*, 5–10 nm in diameter[64]), and it was unlikely that renal excretion would significantly contribute to their blood elimination. Nevertheless, the results confirm that biochemical alterations due to decreased kidney function and/or vascular calcification do not significantly influence how nanoparticles circulate in the bloodstream.

Terminal biodistribution in tissues, 24 h after injection, also shows similar profiles for all animal groups. Here, less than 15% of the injected dose was recovered in the liver, spleen, kidneys, heart, lungs, tibia, and abdominal aorta (Fig. 5). As often with nanomedicines,[61] the nanoparticles were mostly recovered in the liver and the spleen, where 4.5

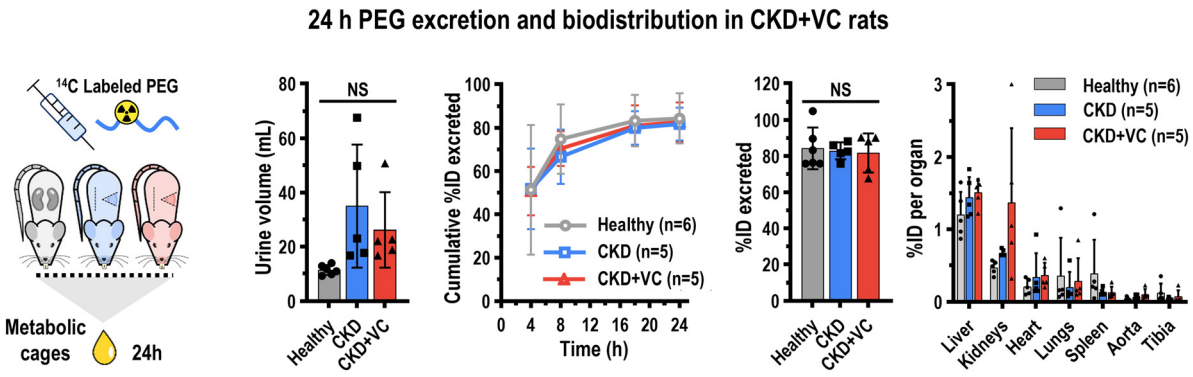

Fig. 4 PEG urinary excretion and biodistribution do not appear to be affected by reduced renal function (CKD) or the presence of vascular calcification (VC). All groups showed no significant difference in the amount of [^{14}C]-PEG excreted and similar excretion profiles. There is no significant difference in the 24 h urine volume between groups. Less than 5% of the injected dose (ID) remains in the tissues analyzed 24 h after [^{14}C]-PEG injection. Values represent mean ± SD for *n* animals. NS: no significant difference ($p > 0.05$ as determined by ANOVA test).

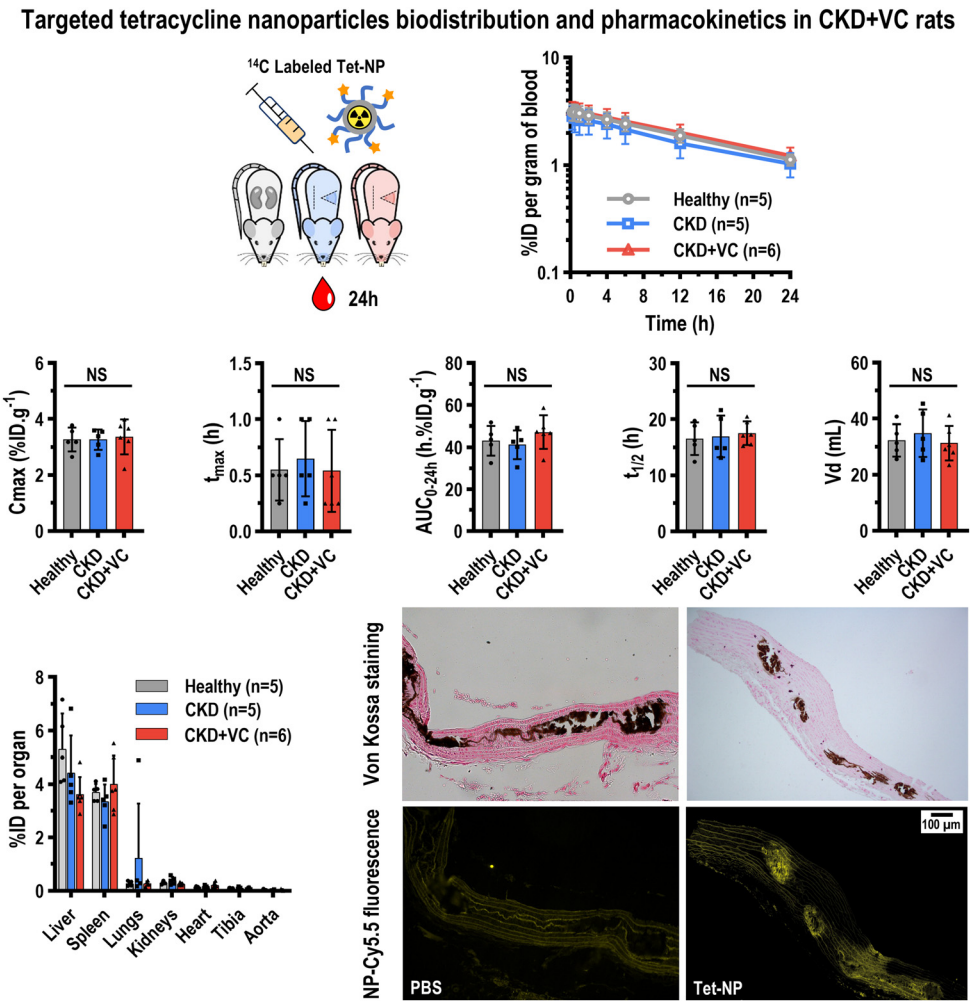

Fig. 5 Targeted tetracycline nanoparticles (Tet-NP) pharmacokinetics (PK) and biodistribution do not appear to be affected by reduced renal function (CKD) or the presence of vascular calcifications (VC). Tet-NP containing 50 wt% of Tet_1-PEG-PLA-polymer and [^{14}C]-PLGA were injected in healthy, CKD and CKD + VC rats and less than 15% of the ID remained in the tissues analyzed, 24 h after Tet-NP injection. The PK profiles were comparable and there was no significant difference between groups for the Tet-NP PK parameters. Cy5.5-labeled Tet-NP (yellow) were preferentially distributed in areas of vascular calcification (dark spots). Values represent mean ± SD for *n* animals. NS: no significant difference ($p > 0.05$ as determined by ANOVA test).

and 3.7% of the injected dose were found, respectively. Interestingly, the amounts of radioactivity recovered in the abdominal aorta and the tibia were not significantly different between groups. This might be because radioactivity is not sensitive enough to detect the minute quantities distributed to these organs or because a significant fraction of the nanoparticles remained in circulation, 24 h after injection. At that time, the last concentration measured was ~1.5% of the injected dose per gram of blood in all groups, which means a total quantity of ~30% of the injected dose was still in circulation when organs were collected (assuming a blood volume equivalent to 7 wt% of the animal).[61] In a parallel study, targeted fluorescent nanoparticles were injected into CKD + VC animals. Here, 24 h after injection, histological analysis of the thoracic aorta showed a signal of fluorescence in the vessel, colocalizing with the vascular calcification plaques (Fig. 5).

3.5 Pharmacokinetics and distribution study of targeted tetracycline nanoparticles loaded with vitamin K in CKD + VC rats

Vitamin K may help prevent vascular calcification in kidney disease, by activating matrix Gla protein (MGP) in vessels, an endogenous calcification inhibitor.[19,20] However, its low oral bioavailability of 10 to 15%[7,65] probably limits its therapeutic efficacy. From a formulation perspective, vitamin K is also attractive because of its hydrophobic nature, which facilitates its encapsulation in the hydrophobic core of nanoparticles.[52,55]

Since nanoparticles are often used as delivery vehicles, we formulated targeted and non-targeted nanoparticles that contained vitamin K (vitamin K1) as a model active molecule. These particles were prepared by nanoprecipitation as described above, with a diameter of 130–150 nm and a PDI

below 0.2. High-performance liquid chromatography (HPLC) analysis of the nanoparticles loaded with vitamin K confirmed a drug-loading content of 8–11 wt% (w/w), across different batches (ESI Table 5†). *In vivo*, both nanoparticles were compared to a control group, a Health Canada-approved emulsion of vitamin K. This formulation contains 10 mg of phytonadione (vitamin K1), 10% polyethylene glycol-15-hydroxystearate, and 2% propylene glycol in 1 mL of water for injection (Phytonadione Injectable Emulsion USP, Sandoz, Boucherville, Canada). Its particle size is 16.64 nm, with a PDI of 0.177, as determined by DLS (ESI Fig. S2†).

CKD + VC rats were randomized to receive one of the three formulations. From a blood sample, we confirmed that all three groups exhibited similar biochemical profiles, with creatinine, phosphate, and calcium levels characteristic of renal impairment (Fig. 6A). Post-mortem analysis also demonstrated similar vascular calcification in all rats, as confirmed by von Kossa staining of aortic tissue (Fig. 6A). For us, these animals represented adequate biological replicates to compare the pharmacokinetic and distribution profiles of vitamin K and the targeted and non-targeted fluorescent nanoparticles.

We dosed all animals with approximately 2.5 mg kg^{-1} of vitamin K (1 mg per animal). Fig. 6B shows the profiles of plasma concentration *vs.* time for free vitamin K (Free K) and vitamin K, encapsulated in non-targeted (NPK), and targeted (Tet-NPK) nanoparticles after intravenous dosing. The pharma-

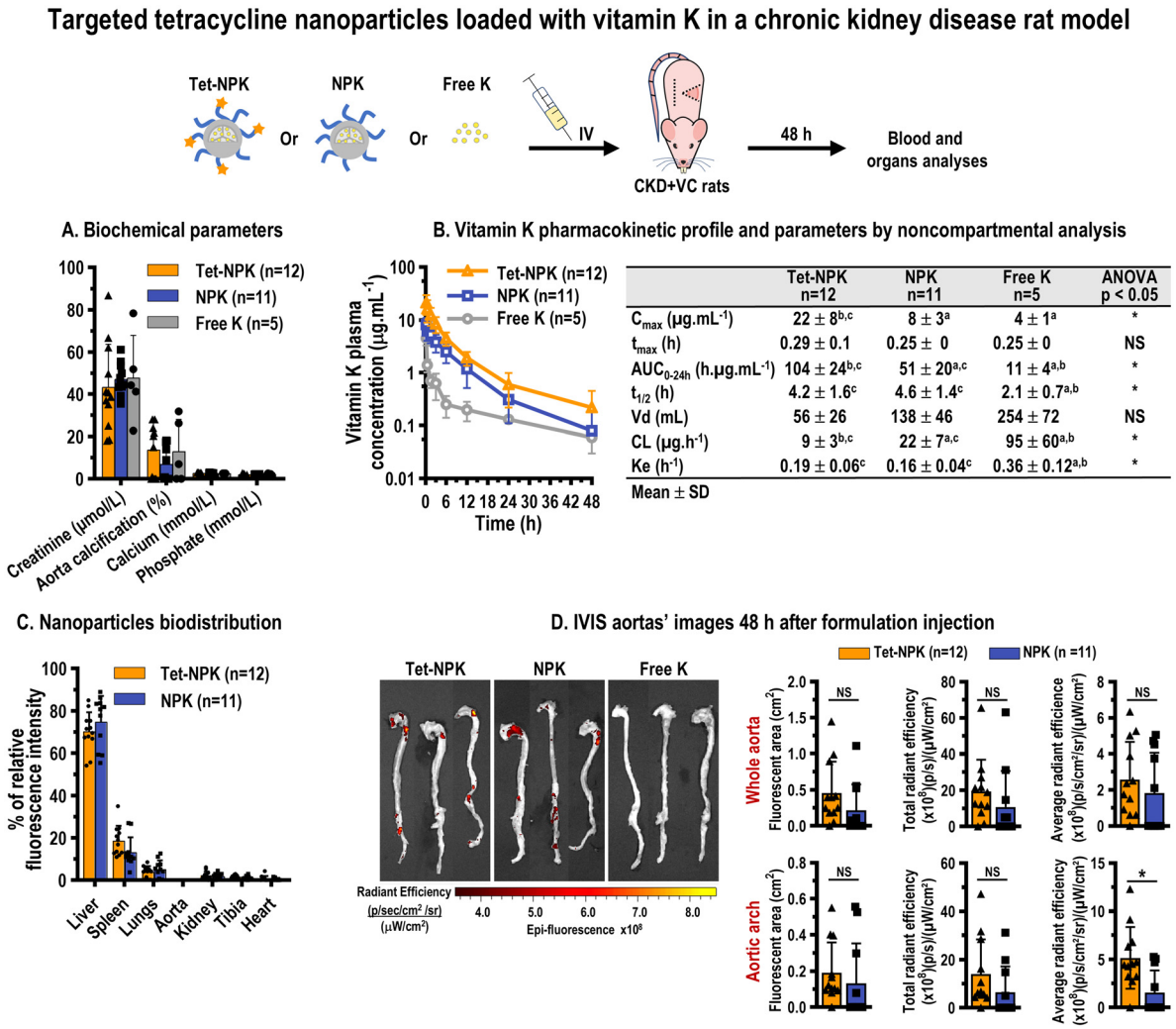

Fig. 6 The encapsulation of vitamin K in targeted nanoparticles (Tet-NP) significantly increases the exposure of the blood compartment to this vitamin. (A) Chronic kidney disease (CKD) induction and vascular calcification (VC) presence were confirmed through blood biochemical analysis and von Kossa staining, respectively. (B) After intravenous injection, the two nanoformulations exhibit distinct pharmacokinetic profiles compared to non-encapsulated vitamin K (Free K). Several pharmacokinetic parameters present significant differences between the groups tested. (C) Targeted (Tet-NPK) and non-targeted (NPK) nanoparticles showed a similar biodistribution profile. (D) Both groups that received nanoparticles showed significantly more fluorescence in the aortas than the group that received the free vitamin K formulation. Values represent mean ± SD from *n* animals. ANOVA with Tukey's *post-hoc* test: $*p < 0.05$. C_{max} maximal concentration; t_{max} maximal concentration time; $AUC_{0-48\ h}$ area under the concentration–time curve from time zero to 48 h; $t_{1/2}$ terminal elimination half-life; V_d volume of distribution; CL total clearance; K_e apparent first-order terminal elimination rate.

cokinetics parameters obtained by non-compartmental analysis are summarized in a table (Fig. 6B). The control group shows that the hydrophobic nature of vitamin K promotes supra-physiological volume of distribution (V_d) and rapid clearance from the bloodstream. This observation is compatible with clinical data from previous studies investigating the pharmacokinetics of intravenous vitamin K in healthy subjects. Shearer *et al.* (1972) reported a half-life ($t_{1/2}$) of 2.3 h for vitamin K when administered as a 1 mg solution in polyethylene glycol.[66] A similar half-life of 2.7 h was observed for a formulation in which vitamin K (6 or 30 μg) was solubilized in mixed micelles composed of glycocholate and lecithin.[67] In both studies, less than 10% of the injected dose remained in the bloodstream 8 h post-administration.[66,67] Similarly, in a preliminary pharmacokinetic study using the abovementioned intravenous micellar formulations, the administration of 2 mg of vitamin K resulted in a high V_d, ranging from 10 to 17 L, with a $t_{1/2}$ between 2.9 and 3.9 h.[68]

In comparison, the encapsulation of vitamin K in Tet-NPK and NPK reduced the V_d and extended its blood exposure. The area under the plasma concentration *vs.* time curve ($AUC_{0-48\ h}$, μg h ml^{-1}) for Tet-NPK and NPK were almost 10- and 5-fold greater than that of free vitamin K, respectively. Half-lives ($t_{1/2}$) in Tet-NPK and in NPK were similar, and approximately 3-fold higher than that of free vitamin K (4.4 *vs.* 1.4, $p < 0.05$ and 3.4 *vs.* 1.4, $p < 0.05$). The higher blood exposure, longer circulation, and the differences in V_d, visible in Fig. 6, together indicate that encapsulation of vitamin K significantly alters its pharmacokinetic profile, irrespective of the presence of targeting ligands. These changes could potentially affect the vitamin's ability to activate MGP in blood vessels, therefore inhibiting the formation of vascular calcification. That said, some differences between nanoparticles were also notable. For example, the maximum concentration (C_{max}) was approximately 3-fold higher for tetracycline-decorated nanoparticles, compared to their non-targeted counterpart. This resulted in a 2-fold difference between the $AUC_{0-48\ h}$ of Tet-NPK, compared to that of NPK. This suggests distinct *in vivo* behavior between targeted and non-targeted nanoparticles, possibly coming from a lower burst release of vitamin K from the tetracycline-containing nanoparticles, as they are introduced into the bloodstream.

To further explore how targeted nanomedicine could reach vascular calcification loci, the nanoparticles described above were prepared with fluorescent Cy5.5-PLA polymer, compatible with IVIS imaging. Specifically, we measured tissue fluorescence in the primary organs (liver, spleen, lungs, kidneys, and heart), as well as in the aorta and tibia, 48 h following the intravenous administration of Tet-NPK and NPK. The percentages of relative fluorescence intensity, normalized by the summation of total radiant efficiency detected in all tissues, is shown in Fig. 6C. Biodistribution profiles were comparable between targeted and non-targeted particles. As anticipated (and consistent with results presented in Fig. 5), both particle types exhibited greater accumulation in the primary organs of the mononuclear phagocyte system, specifically the liver and spleen.

Specifically for the aortas, IVIS imaging revealed the presence of fluorescent loci in the groups that received nanoparticles, and some differences in fluorescence were appreciated between the aortas collected from animals that received targeted and non-targeted nanoparticles (Fig. 6D). No fluorescence was detectable in the tissues of animals that received free vitamin K (all aorta images are available in ESI Fig. S6†). When focusing on the whole thoracic aorta, fluorescence was detected in 11/12 animals that received Tet-NPK, compared to 5/10 animals that received non-targeted nanoparticles. The area covered by the fluorescent signal (in cm^2) was approximately 2-fold higher in the targeted group, but the large variability between individuals made this difference non-statistically significant. Similar results were obtained when comparing the total and average radiant efficiency, which were respectively 1.4- and 1.9-fold higher in the Tet-NPK group (without statistical differences). These measurements represent the cumulative intensity of the fluorescence signal detected in the tissue, and the average fluorescent signal normalized per unit of area – respectively, they represent '*how much*' nanoparticles remain in the tissue, and '*how densely localized*' is the fluorescence. When focusing only on the aortic arch, which is an anatomical region with high risk of calcification, 11/12 animals had detectable fluorescence in the Tet-NPK group, compared to 4/10 in the NPK group. Again, the fluorescent area and total radiant efficiency were 1.4- and 2.1-fold higher in the targeted group, but differences were not statistically significant. Only the average fluorescence intensity indicated that tetracycline-functionalized nanoparticles distributed more densely to the aortic cross, compared to their non-targeted counterpart. Finally, we also measured the concentrations of vitamin K in the aortas by HPLC (ESI Fig. S4†). In this analysis, no differences were noted between both types of nanoparticle. Unexpectedly, the concentrations of vitamin K in the group that received the emulsion (control) were higher than those observed with nanoparticles. The reasons behind this observation remain unclear. However, because vitamin K is fat-soluble, it is possible that, after an intravenous bolus, the free molecule can diffuse deeper and more extensively in the vascular tissue than its encapsulated form. If so, further work will investigate if the differentiated pharmacology resulting from the slow release of the drug from the nanoparticles might be more beneficial for other molecules, with physicochemical properties that are distinct from those of vitamin K.

Together, these results suggest that, in the conditions tested, functionalization of nanoparticles with tetracycline does not drastically alter the distribution of nanoparticles to calcified aortas, 48 h after injection. This contrasts with the semi-quantitative histological indications presented in Fig. 5, which show colocalization of the nanoparticle fluorescent signal with VC. Multiple explanations can contextualize these observations. The aorta is the vessel where the blood flow is the fastest. The negligible differences between targeted and non-targeted formulations suggest that the affinity of the ligand for hydroxyapatite is not sufficient to significantly alter the deposition of the nanoparticles, in these conditions. The

high blood flow might hinder tetracycline–hydroxyapatite interactions from happening or wash away the nanoparticles that initially deposit to the vascular wall. Furthermore, we have recently shown that fluorescent dyes conjugated to the terminal end of PLA chains can hydrolyze *in vivo*.[53] It is possible that over 48 h, polymer degradation releases the fluorescent signal, decreasing our ability to confirm the presence of the nanoparticles in the tissue. Likewise, since targeted and non-targeted formulations have similar circulation times, the amounts of non-targeted nanoparticles remaining in the blood after 48 h may contribute to a background signal that obscures our ability to quantify distribution to vascular calcification plaques by IVIS imaging. In the present study, due to technical limitations, it was not possible to analyze the exact same biospecimens by IVIS imaging, HPLC dosing, and histology in parallel, and further studies will be necessary to fully elucidate how functionalization with tetracycline can be used in the context of vascular calcification.

4. Conclusion

In this study, we investigated the pharmacology of tetracycline-functionalized nanoparticles in animals with chronic kidney disease (CKD), with and without vascular calcification. These formulations had an interest, due to their documented ability to target hydroxyapatite. We demonstrated that PEG excretion, as well as the pharmacokinetic profile and biodistribution of tetracycline-functionalized nanoparticles, are not affected by CKD or the presence of vascular calcification. As nanomedicines are increasingly investigated to treat chronic diseases, this information is important to inform on the pharmacology of nanoparticles in different contexts.

In animals with CKD and vascular calcification, we were able to show that encapsulation of vitamin K, a model hydrophobic molecule, significantly altered its pharmacokinetic profile. This information might be valuable in conditions where increased blood exposure can improve a drug's pharmacological effects. Nevertheless, post-mortem analysis of tissues, conducted with current methodological limitations, did not provide convincing evidence of the ability of tetracycline functionalization to significantly alter the deposition of nanoparticles to the vascular wall, compared to non-targeted nanoparticles. At this stage, it is difficult to ascertain if the absence of differences between formulations is due to a conceptual flaw or to technical limitations. Although the formulation approach is simple and robust, and allows the efficient encapsulation of vitamin K, further work will be necessary to fully elucidate the potential of tetracycline functionalization on the targeting of vascular calcification. Non-targeted, injectable vitamin K formulations are already available on the market. Therefore, a novel vitamin K nanomedicine technology would require undeniable benefits over existing products to warrant further (pre)clinical development. Future studies will be necessary to evaluate if the differentiated pharmacokinetics presented herein with targeted and non-targeted nanoparticles translate into improved efficacy to revert vascular calcification, without raising safety considerations. Overall, we believe that this work clarifies our understanding of the potential of nanomedicines in the treatment of kidney disease complications and offers fundamental information that will eventually contribute to the development of technologies that can benefit patients.

Author contributions

VDPM – conceptualization, methodology, investigation, formal analysis, visualization, writing – original draft. RVU – investigation, writing – review and editing. KG – investigation, writing – review and editing. SP – investigation, writing – review and editing. NG – investigation, writing – review and editing. FMW – conceptualization, funding acquisition, writing – review and editing. NB – conceptualization, methodology, funding acquisition, formal analysis, project administration, writing – review and editing.

Conflicts of interest

The authors declare no conflict of interest with regard to the research presented in this manuscript.

Data availability

The data supporting this article have been included as part of the ESI.†

Acknowledgements

This work was funded by a grant from the Kidney Foundation of Canada (FMW and NB, reference 674775-2020), the Natural Sciences and Engineering Research Council of Canada (NSERC, NB, reference RGPIN-2023-05349). Infrastructure was supported by grants from the Canadian Funds for Innovation (CFI, NB, reference 35981 and 43725), and the Fonds de recherche du Québec (FRQ) through a grant to the CHU de Québec-Université Laval Research Center (reference: 30641). Vanessa D. P. Maio and Nicolas Gaudreault have received fellowships from the Fonds de Recherche du Québec – Nature et Technologies (FRQNT), the Fonds d'Enseignement et de Recherche of the Faculty of Pharmacy at Université Laval, and the Fondation du CHU de Québec. Nicolas Bertrand and Fabrice Mac-Way are Research Scholars (Junior 2 and Senior) from the Fonds de Recherche du Québec – Santé (FRQS).

References

1 L. P. Gregg and S. S. Hedayati, Management of Traditional Cardiovascular Risk Factors in CKD: What Are the Data?,

Am. J. Kidney Dis., 2018, **72**(5), 728–744, DOI: 10.1053/j.ajkd.2017.12.007.

2 A. Ortiz, A. Covic, D. Fliser, D. Fouque, D. Goldsmith, M. Kanbay, F. Mallamaci, Z. A. Massy, P. Rossignol, R. Vanholder, *et al.*, Epidemiology, contributors to, and clinical trials of mortality risk in chronic kidney failure, *Lancet*, 2014, **383**(9931), 1831–1843, DOI: 10.1016/S0140-6736(14)60384-6.

3 C. Vachey, A. Candellier, S. Toutain and F. Mac-Way, The Bone-Vascular Axis in Chronic Kidney Disease: From Pathophysiology to Treatment, *Curr. Osteoporos. Rep.*, 2024, **22**(1), 69–79, DOI: 10.1007/s11914-023-00858-8.

4 J. Jankowski, J. Floege, D. Fliser, M. Böhm and N. Marx, Cardiovascular Disease in Chronic Kidney Disease: Pathophysiological Insights and Therapeutic Options, *Circulation*, 2021, **143**(11), 1157–1172, DOI: 10.1161/circulationaha.120.050686.

5 P. Romagnani, G. Remuzzi, R. Glassock, A. Levin, K. J. Jager, M. Tonelli, Z. Massy, C. Wanner and H.-J. Anders, Chronic kidney disease, *Nat. Rev. Dis. Primers*, 2017, **3**(1), 17088, DOI: 10.1038/nrdp.2017.88.

6 E. Kakani, M. Elyamny, T. Ayach and A. El-Husseini, Pathogenesis and management of vascular calcification in CKD and dialysis patients, *Semin. Dial.*, 2019, **32**(6), 553–561, DOI: 10.1111/sdi.12840.

7 A. C. Akbulut, A. Pavlic, P. Petsophonsakul, M. Halder, K. Maresz, R. Kramann and L. Schurgers, Vitamin K2 Needs an RDI Separate from Vitamin K1, *Nutrients*, 2020, **12**(6), 1852, DOI: 10.3390/nu12061852.

8 P. A. Price, A. M. Roublick and M. K. Williamson, Artery calcification in uremic rats is increased by a low protein diet and prevented by treatment with ibandronate, *Kidney Int.*, 2006, **70**(9), 1577–1583, DOI: 10.1038/sj.ki.5001841.

9 K. Tamura, Y. Suzuki, H. Hashiba, H. Tamura, S. Aizawa and H. Kogo, Effect of etidronate on aortic calcification and bone metabolism in calcitriol-treated rats with subtotal nephrectomy, *J. Pharmacol. Sci.*, 2005, **99**(1), 89–94.

10 G. Kranenburg, J. W. Bartstra, M. Weijmans, P. A. de Jong, W. P. Mali, H. J. Verhaar, F. L. J. Visseren and W. Spiering, Bisphosphonates for cardiovascular risk reduction: A systematic review and meta-analysis, *Atherosclerosis*, 2016, **252**, 106–115.

11 E. J. Samelson, P. D. Miller, C. Christiansen, N. S. Daizadeh, L. Grazette, M. S. Anthony, O. Egbuna, A. Wang, S. R. Siddhanti, A. M. Cheung, *et al.*, RANKL inhibition with denosumab does not influence 3-year progression of aortic calcification or incidence of adverse cardiovascular events in postmenopausal women with osteoporosis and high cardiovascular risk, *J. Bone Miner. Res.*, 2014, **29**(2), 450–457, DOI: 10.1002/jbmr.2043.

12 S. Helas, C. Goettsch, M. Schoppet, U. Zeitz, U. Hempel, H. Morawietz, P. J. Kostenuik, R. G. Erben and L. C. Hofbauer, Inhibition of receptor activator of NF-kappaB ligand by denosumab attenuates vascular calcium deposition in mice, *Am. J. Pathol.*, 2009, **175**(2), 473–478, DOI: 10.2353/ajpath.2009.080957.

13 H. Fleisch, Bisphosphonates: mechanisms of action, *Endocr. Rev.*, 1998, **19**(1), 80–100, DOI: 10.1210/edrv.19.1.0325.

14 S. Panizo, A. Cardus, M. Encinas, E. Parisi, P. Valcheva, S. López-Ongil, B. Coll, E. Fernandez and J. M. Valdivielso, RANKL increases vascular smooth muscle cell calcification through a RANK-BMP4-dependent pathway, *Circ. Res.*, 2009, **104**(9), 1041–1048, DOI: 10.1161/CIRCRESAHA.108.189001.

15 J. J. Kaden, S. Bickelhaupt, R. Grobholz, K. K. Haase, A. Sarikoç, R. Kiliç, M. Brueckmann, S. Lang, I. Zahn, C. Vahl, *et al.*, Receptor activator of nuclear factor kappaB ligand and osteoprotegerin regulate aortic valve calcification, *J. Mol. Cell Cardiol.*, 2004, **36**(1), 57–66, DOI: 10.1016/j.yjmcc.2003.09.015.

16 C. F. Marlow, S. Sharma, F. Babar and J. Lin, Severe Hypocalcemia and Hypomagnesemia with Denosumab in Advanced Chronic Kidney Disease: Case Report and Literature Review, *Case Rep. Oncol. Med.*, 2018, **2018**, 2059364, DOI: 10.1155/2018/2059364.

17 S. Suzuki, M. Suzuki, N. Hanafusa, K. Tsuchiya and K. Nitta, Denosumab Recovers Aortic Arch Calcification During Long-Term Hemodialysis, *Kidney Int. Rep.*, 2020, **6**(3), 605–612, DOI: 10.1016/j.ekir.2020.12.002.

18 M. Cozzolino, F. Maffei Faccioli, A. Cara, G. Boni Brivio, F. Rivela, P. Ciceri, L. Magagnoli, A. Galassi, S. Barbuto, S. Speciale, *et al.*, Future treatment of vascular calcification in chronic kidney disease, *Expert Opin. Pharmacother.*, 2023, **24**(18), 2041–2057, DOI: 10.1080/14656566.2023.2266381.

19 G. Luo, P. Ducy, M. D. McKee, G. J. Pinero, E. Loyer, R. R. Behringer and G. Karsenty, Spontaneous calcification of arteries and cartilage in mice lacking matrix GLA protein, *Nature*, 1997, **386**(6620), 78–81, DOI: 10.1038/386078a0.

20 M. K. Shea, C. J. O'Donnell, U. Hoffmann, G. E. Dallal, B. Dawson-Hughes, J. M. Ordovas, P. A. Price, M. K. Williamson and S. L. Booth, Vitamin K supplementation and progression of coronary artery calcium in older men and women, *Am. J. Clin. Nutr.*, 2009, **89**(6), 1799–1807, DOI: 10.3945/ajcn.2008.27338.

21 I. E. Neofytou, A. Stamou, A. Demopoulos, S. Roumeliotis, P. Zebekakis, V. Liakopoulos, E. Stamellou and E. Dounousi, Vitamin K for Vascular Calcification in Kidney Patients: Still Alive and Kicking, but Still a Lot to Learn, *Nutrients*, 2024, **16**(12), 1798, DOI: 10.3390/nu16121798.

22 L. J. Schurgers, D. V. Barreto, F. C. Barreto, S. Liabeuf, C. Renard, E. J. Magdeleyns, C. Vermeer, G. Choukroun and Z. A. Massy, The circulating inactive form of matrix gla protein is a surrogate marker for vascular calcification in chronic kidney disease: a preliminary report, *Clin. J. Am. Soc. Nephrol.*, 2010, **5**(4), 568–575, DOI: 10.2215/cjn.07081009.

23 S. Roumeliotis, E. Dounousi, T. Eleftheriadis and V. Liakopoulos, Association of the Inactive Circulating

Matrix Gla Protein with Vitamin K Intake, Calcification, Mortality, and Cardiovascular Disease: A Review, *Int. J. Mol. Sci.*, 2019, **20**(3), 628, DOI: 10.3390/ijms20030628.

24 L. J. Schurgers, H. M. Spronk, B. A. Soute, P. M. Schiffers, J. G. DeMey and C. Vermeer, Regression of warfarin-induced medial elastocalcinosis by high intake of vitamin K in rats, *Blood*, 2007, **109**(7), 2823–2831, DOI: 10.1182/blood-2006-07-035345.

25 C. Geng, L. Huang, L. Pu and Y. Feng, Effects of vitamin K supplementation on vascular calcification in chronic kidney disease: A systematic review and meta-analysis of randomized controlled trials, *Front. Nutr.*, 2022, **9**, 1001826, DOI: 10.3389/fnut.2022.1001826.

26 C. Xu, E. R. Smith, M. K. Tiong, I. Ruderman and N. D. Toussaint, Interventions To Attenuate Vascular Calcification Progression in Chronic Kidney Disease: A Systematic Review of Clinical Trials, *J. Am. Soc. Nephrol.*, 2022, **33**(5), 1011–1032, DOI: 10.1681/asn.2021101327.

27 M. Marinova, D. Lütjohann, O. Breuer, H. Kölsch, P. Westhofen, M. Watzka, M. Mengel, B. Stoffel-Wagner, G. Hartmann, C. Coch, *et al.*, VKORC1-dependent pharmacokinetics of intravenous and oral phylloquinone (vitamin K1) mixed micelles formulation, *Eur. J. Clin. Pharmacol.*, 2013, **69**(3), 467–475, DOI: 10.1007/s00228-012-1362-y.

28 N.-J. Chiang, J.-Y. Chang, Y.-S. Shan and L.-T. Chen, Development of nanoliposomal irinotecan (nal-IRI, MM-398, PEP02) in the management of metastatic pancreatic cancer, *Expert Opin. Pharmacother.*, 2016, **17**(10), 1413–1420.

29 Y. H. Song, E. Shin, H. Wang, J. Nolan, S. Low, D. Parsons, S. Zale, S. Ashton, M. Ashford, M. Ali, *et al.*, A novel in situ hydrophobic ion pairing (HIP) formulation strategy for clinical product selection of a nanoparticle drug delivery system, *J. Controlled Release*, 2016, **229**, 106–119, DOI: 10.1016/j.jconrel.2016.03.026.

30 M. E. Davis, J. E. Zuckerman, C. H. Choi, D. Seligson, A. Tolcher, C. A. Alabi, Y. Yen, J. D. Heidel and A. Ribas, Evidence of RNAi in humans from systemically administered siRNA via targeted nanoparticles, *Nature*, 2010, **464**(7291), 1067–1070, DOI: 10.1038/nature08956.

31 J. Hrkach, D. Von Hoff, M. M. Ali, E. Andrianova, J. Auer, T. Campbell, D. De Witt, M. Figa, M. Figueiredo, A. Horhota, *et al.*, Preclinical development and clinical translation of a PSMA-targeted docetaxel nanoparticle with a differentiated pharmacological profile, *Sci. Transl. Med.*, 2012, **4**(128), 128ra139, DOI: 10.1126/scitranslmed.3003651.

32 D. D. Von Hoff, M. M. Mita, R. K. Ramanathan, G. J. Weiss, A. C. Mita, P. M. LoRusso, H. A. Burris, 3rd, L. L. Hart, S. C. Low, D. M. Parsons, *et al.* Phase I Study of PSMA-Targeted Docetaxel-Containing Nanoparticle BIND-014 in Patients with Advanced Solid Tumors, *Clin. Cancer Res.*, 2016, **22**(13), 3157–3163, DOI: 10.1158/1078-0432.CCR-15-2548.

33 A. J. Mieszawska, W. J. M. Mulder, Z. A. Fayad and D. P. Cormode, Multifunctional Gold Nanoparticles for Diagnosis and Therapy of Disease, *Mol. Pharm.*, 2013, **10**(3), 831–847, DOI: 10.1021/mp3005885.

34 J. Song, N. Cui, X. Mao, Q. Huang, E. S. Lee and H. Jiang, Sorption Studies of Tetracycline Antibiotics on Hydroxyapatite (001) Surface-A First-Principles Insight, *Materials*, 2022, **15**(3), 797, DOI: 10.3390/ma15030797.

35 F. Lavigne, L. C. Desbiens, G. Garneau, F. Côté and F. Mac-Way, Iliac crest bone biopsy by interventional radiologists to improve access to bone biopsy in chronic kidney disease populations: technical note and a case series, *J. Nephrol.*, 2021, **34**(3), 901–906, DOI: 10.1007/s40620-020-00798-x.

36 S. K. Bisson, R. V. Ung, S. Picard, D. Valade, M. Agharazii, R. Lariviere and F. Mac-Way, High calcium, phosphate and calcitriol supplementation leads to an osteocyte-like phenotype in calcified vessels and bone mineralisation defect in uremic rats, *J. Bone Miner. Metab.*, 2019, **37**(2), 212–223, DOI: 10.1007/s00774-018-0919-y.

37 S. Moe, T. Drüeke, J. Cunningham, W. Goodman, K. Martin, K. Olgaard, S. Ott, S. Sprague, N. Lameire and G. Eknoyan, Definition, evaluation, and classification of renal osteodystrophy: A position statement from Kidney Disease: Improving Global Outcomes (KDIGO), *Kidney Int.*, 2006, **69**(11), 1945–1953, DOI: 10.1038/sj.ki.5000414.

38 H. Wang, J. Liu, S. Tao, G. Chai, J. Wang, F.-Q. Hu and H. Yuan, Tetracycline-grafted PLGA nanoparticles as bone-targeting drug delivery system, *Int. J. Nanomed.*, 2015, **10**, 5671–5685, DOI: 10.2147/IJN.S88798 PubMed.

39 J. Wang, S. Tao, X. Jin, Y. Song, W. Zhou, H. Lou, R. Zhao, C. Wang, F. Hu and H. Yuan, Calcium Supplement by Tetracycline guided amorphous Calcium Carbonate potentiates Osteoblast promotion for Synergetic Osteoporosis Therapy, *Theranostics*, 2020, **10**(19), 8591–8605, DOI: 10.7150/thno.45142.

40 Y. Que, Y. Yang, H. Zafar and D. Wang, Tetracycline-grafted mPEG-PLGA micelles for bone-targeting and osteoporotic improvement, *Front. Pharmacol.*, 2022, **13**, 993095, DOI: 10.3389/fphar.2022.993095.

41 Q. Liang, P. Zhang, L. Zhang, H. Luan, X. Li, H. Xiang, S. Jing and X. Song, Development of tetracycline-modified nanoparticles for bone-targeted delivery of anti-tubercular drug, *Front. Bioeng. Biotechnol*, 2023, **11**, 1207520, DOI: 10.3389/fbioe.2023.1207520.

42 N. Bertrand, P. Grenier, M. Mahmoudi, E. M. Lima, E. A. Appel, F. Dormont, J. M. Lim, R. Karnik, R. Langer and O. C. Farokhzad, Mechanistic understanding of in vivo protein corona formation on polymeric nanoparticles and impact on pharmacokinetics, *Nat. Commun.*, 2017, **8**, 8, DOI: 10.1038/s41467-017-00600-w.

43 J. M. Chan, L. Zhang, R. Tong, D. Ghosh, W. Gao, G. Liao, K. P. Yuet, D. Gray, J.-W. Rhee, J. Cheng, *et al.*, Spatiotemporal controlled delivery of nanoparticles to injured vasculature, *Proc. Natl. Acad. Sci. U. S. A.*, 2010, **107**(5), 2213–2218, DOI: 10.1073/pnas.0914585107.

44 D. D. Chin, J. Wang, M. Mel de Fontenay, A. Plotkin, G. A. Magee and E. J. Chung, Hydroxyapatite-binding micelles for the detection of vascular calcification in ather-

osclerosis, *J. Mater. Chem. B*, 2019, **7**(41), 6449–6457, DOI: 10.1039/c9tb01918a.

45 Y. Lei, N. Nosoudi and N. Vyavahare, Targeted chelation therapy with EDTA-loaded albumin nanoparticles regresses arterial calcification without causing systemic side effects, *J. Controlled Release*, 2014, **196**, 79–86, DOI: 10.1016/j.jconrel.2014.09.029.

46 A. Sinha, A. Shaporev, N. Nosoudi, Y. Lei, A. Vertegel, S. Lessner and N. C. B. Vyavahare, Nanoparticle targeting to diseased vasculature for imaging and therapy, *Nanomedicine*, 2014, **10**(5), e1003–e1012, DOI: 10.1016/j.nano.2014.02.002.

47 S. R. Karamched, N. Nosoudi, H. E. Moreland, A. Chowdhury and N. R. Vyavahare, Site-specific chelation therapy with EDTA-loaded albumin nanoparticles reverses arterial calcification in a rat model of chronic kidney disease, *Sci. Rep.*, 2019, **9**(1), 2629, DOI: 10.1038/s41598-019-39639-8.

48 N. Bertrand, J. Wu, X. Xu, N. Kamaly and O. C. Farokhzad, Cancer nanotechnology: The impact of passive and active targeting in the era of modern cancer biology, *Adv. Drug Delivery Rev.*, 2014, **66**, 2–25, DOI: 10.1016/j.addr.2013.11.009.

49 F. Brandl, N. Bertrand, E. M. Lima and R. Langer, Nanoparticles with photoinduced precipitation for the extraction of pollutants from water and soil, *Nat. Commun.*, 2015, **6**, 10, DOI: 10.1038/ncomms8765.

50 J. Cheng, B. A. Teply, I. Sherifi, J. Sung, G. Luther, F. X. Gu, E. Levy-Nissenbaum, A. F. Radovic-Moreno, R. Langer and O. C. Farokhzad, Formulation of functionalized PLGA–PEG nanoparticles for in vivo targeted drug delivery, *Biomaterials*, 2007, **28**(5), 869–876, DOI: 10.1016/j.biomaterials.2006.09.047.

51 A. Dikpati, F. Mohammadi, K. Greffard, C. Quéant, P. Arnaud, G. Bastiat, I. Rudkowska and N. Bertrand, Residual Solvents in Nanomedicine and Lipid-Based Drug Delivery Systems: a Case Study to Better Understand Processes, *Pharm. Res.*, 2020, **37**(8), 149, DOI: 10.1007/s11095-020-02877-x.

52 Y. C. Hacene, A. Loiseau, V. D. P. Maio, P. Grenier, E. Boisselier and N. Bertrand, Isolating Nanoparticles from Complex Biological Media by Immunoprecipitation, *Nano Lett.*, 2021, **21**(11), 4530–4538, DOI: 10.1021/acs.nanolett.0c05056.

53 S. Roussel, P. Grenier, V. Chénard and N. Bertrand, Dual-Labelled Nanoparticles Inform on the Stability of Fluorescent Labels In Vivo, *Pharmaceutics*, 2023, **15**(3), 769, DOI: 10.3390/pharmaceutics15030769.

54 J. M. Gregoire, L. Zhou and J. A. Haber, Combinatorial synthesis for AI-driven materials discovery, *Nat. Synth.*, 2023, **2**(6), 493–504, DOI: 10.1038/s44160-023-00251-4.

55 A. Dikpati, V. D. P. Maio, E. Ates, K. Greffard and N. Bertrand, Studying the stability of polymer nanoparticles by size exclusion chromatography of radioactive polymers, *J. Controlled Release*, 2024, **369**, 394–403, DOI: 10.1016/j.jconrel.2024.03.053.

56 J. Herrmann, M. Babic, M. Tölle, M. van der Giet and M. Schuchardt, Research Models for Studying Vascular Calcification, *Int. J. Mol. Sci.*, 2020, **21**(6), 2204, DOI: 10.3390/ijms21062204.

57 A. Gauthier-Bastien, R. V. Ung, R. Lariviere, F. Mac-Way, M. Lebel and M. Agharazii, Vascular remodeling and media calcification increases arterial stiffness in chronic kidney disease, *Clin. Exp. Hypertens.*, 2014, **36**(3), 173–180, DOI: 10.3109/10641963.2013.804541.

58 R. Larivière, R. V. Ung, S. Picard, D. E. Richard, F. Mac-Way and M. Agharazii, Antihypertensive treatment with hydrochlorothiazide-hydralazine combination aggravates medial vascular calcification in CKD rats with mineral bone disorder, *Front. Cardiovasc. Med.*, 2023, **10**, 1241943, DOI: 10.3389/fcvm.2023.1241943.

59 G. O. Ferrari, J. C. Ferreira, R. T. Cavallari, K. R. Neves, L. M. dos Reis, W. V. Dominguez, E. C. Oliveira, F. G. Graciolli, J. Passlick-Deetjen, V. Jorgetti, *et al.*, Mineral bone disorder in chronic kidney disease: head-to-head comparison of the 5/6 nephrectomy and adenine models, *BMC Nephrol.*, 2014, **15**(1), 69, DOI: 10.1186/1471-2369-15-69.

60 M. Ketteler, G. A. Block, P. Evenepoel, M. Fukagawa, C. A. Herzog, L. McCann, S. M. Moe, R. Shroff, M. A. Tonelli, N. D. Toussaint, *et al.*, Executive summary of the 2017 KDIGO Chronic Kidney Disease-Mineral and Bone Disorder (CKD-MBD) Guideline Update: what's changed and why it matters, *Kidney Int.*, 2017, **92**(1), 26–36, DOI: 10.1016/j.kint.2017.04.006.

61 N. Bertrand and J. C. Leroux, The journey of a drug-carrier in the body: An anatomo-physiological perspective, *J. Controlled Release*, 2012, **161**(2), 152–163, DOI: 10.1016/j.jconrel.2011.09.098.

62 T. Yamaoka, Y. Tabata and Y. Ikada, Distribution and tissue uptake of poly(ethylene glycol) with different molecular weights after intravenous administration to mice, *J. Pharm. Sci.*, 1994, **83**(4), 601–606, DOI: 10.1002/jps.2600830432.

63 P. Grenier, I. M. D. Viana, E. M. Lima and N. Bertrand, Anti-polyethylene glycol antibodies alter the protein corona deposited on nanoparticles and the physiological pathways regulating their fate in vivo, *J. Controlled Release*, 2018, **287**, 121–131, DOI: 10.1016/j.jconrel.2018.08.022.

64 H. S. Choi, W. Liu, P. Misra, E. Tanaka, J. P. Zimmer, B. Itty Ipe, M. G. Bawendi and J. V. Frangioni, Renal clearance of quantum dots, *Nat. Biotechnol.*, 2007, **25**(10), 1165–1170, DOI: 10.1038/nbt1340.

65 L. J. Schurgers, K. J. Teunissen, K. Hamulyák, M. H. Knapen, H. Vik and C. Vermeer, Vitamin K-containing dietary supplements: comparison of synthetic vitamin K1 and natto-derived menaquinone-7, *Blood*, 2007, **109**(8), 3279–3283, DOI: 10.1182/blood-2006-08-040709.

66 M. J. Shearer, C. N. Mallinson, G. R. Webster and P. Barkhan, Clearance from Plasma and Excretion in Urine, Faeces and Bile of an Intravenous Dose of Tritiated Vitamin K1 in Man, *Br. J. Haematol.*, 1972, **22**(5), 579–588, DOI: 10.1111/j.1365-2141.1972.tb05704.x.

67 K. S. Jones, L. J. Bluck, L. Y. Wang and W. A. Coward, A stable isotope method for the simultaneous measurement of vitamin K1 (phylloquinone) kinetics and absorption, *Eur. J. Clin. Nutr.*, 2008, **62**(11), 1273–1281, DOI: **10.1038/sj.ejcn.1602859**.

68 M. Marinova, D. Lütjohann, P. Westhofen, M. Watzka, O. Breuer and J. Oldenburg, A Validated HPLC Method for the Determination of Vitamin K in Human Serum – First Application in a Pharmacological Study, *Open Clin. Chem. J.*, 2011, **4**, 17–27.